

## 基于自适应 EKF 的摄像机标定优化方法

赖欣<sup>1,2</sup>, 杨肖<sup>2</sup>, 张启灿<sup>1\*</sup><sup>1</sup>四川大学电子信息学院, 四川 成都 610065;<sup>2</sup>西南石油大学机电工程学院, 四川 成都 610500

**摘要** 针对扩展卡尔曼滤波算法在摄像机标定优化应用中, 滤波精度较大程度地依赖于噪声协方差矩阵的准确性这一问题, 提出了一种基于自适应扩展卡尔曼滤波算法的摄像机标定优化方法。以所检测到的二维棋盘格靶上特征点的图像坐标作为自适应扩展卡尔曼滤波算法的观测量, 摄像机的内、外参数作为状态量, 将观测图像上的特征点进行逐点滤波运算, 过程和观测噪声协方差矩阵在迭代过程中随着观测值和预测值之间新息的变化而更新, 从而优化对应的摄像机参数。实验结果表明, 经本文算法优化后获得的摄像机内、外参数具有较小的重投影误差, USB 相机和工业相机的标定结果较张正友标定法分别提升了 61.17% 和 12.17%, 所提算法较无迹卡尔曼滤波算法和扩展卡尔曼滤波算法在噪声环境下具有更高的标定精度和更好的鲁棒性。

**关键词** 机器视觉; 摄像机标定; 扩展卡尔曼滤波; 新息; 自适应; 重投影误差

**中图分类号** TP391 **文献标志码** A

**DOI:** 10.3788/AOS231144

## 1 引言

摄像机标定是机器视觉应用过程中的一个重要步骤, 即获取摄像机成像过程中从三维空间已知特征点到与之对应的二维图像信息的摄像机参数, 摄像机标定参数包括摄像机的内部参数和外部参数<sup>[1-5]</sup>。摄像机标定是三维重建、缺陷检测、视觉导航、机器人定位、姿态估计、视频监控和医疗诊断<sup>[6-10]</sup>等方面的必要环节, 同时, 在实际应用过程中, 摄像机标定的精度往往直接决定整个视觉系统的精度和性能。

相机标定方法主要有传统相机标定法、主动视觉相机标定法和相机自标定法<sup>[11-13]</sup>。为了获取更高精度的摄像机标定参数, 广大学者对摄像机标定进行了大量的研究, 也提出了一些成熟的标定方法, 其中最常用的是由张正友提出的基于 2D 平面靶的摄像机标定法<sup>[14]</sup>。卡尔曼滤波算法是一种最优估计算法, 利用前一时刻的预测值和当前时刻的观测值对状态量进行准确预测, 提供了一种高效可计算的方法来估计过程的状态, 可以应用于摄像机标定领域。Tommaselli 等<sup>[15]</sup>以平面上沿线性轨迹运动的立方体作为标定靶进行动态拍摄, 通过将上一时刻所拍摄图像中的特征经过系统模型获得下一时刻图像特征的先验估计, 完成了摄像机的动态标定; Stringa 等<sup>[16]</sup>在视频监控的摄像机标定中, 将一个已知几何形状的物体作为标定靶, 仅对目

标上一点进行三维测量, 利用扩展卡尔曼滤波(EKF)算法和标靶的已知几何形状, 对标靶的其他目标点进行估计, 完成了摄像机外部参数的标定。以上两种标定方法都是采用三维立体标定靶, 由于制作成本和加工精度等问题在应用过程中受到了很大的限制。陈益等<sup>[17]</sup>将无迹卡尔曼滤波(UKF)算法应用在了摄像机标定中, 并采用简化无迹卡尔曼(SUKF)降低运算复杂度, 提高了计算效率。Zhou 等<sup>[18-19]</sup>提出了基于扩展卡尔曼滤波算法和二维标靶的摄像机标定应用, 取得了较好的标定效果。EKF 对影响摄像机标定参数优化效果的过程噪声和观测噪声的初值设定一般依赖于用户的经验, 存在一定的局限性, 使用自适应算法对扩展卡尔曼滤波中的过程和观测噪声协方差矩阵进行更新具有更大优越性<sup>[20-21]</sup>。

本文针对 EKF 在各种应用场景下无法自动选择和调整摄像机标定中的过程噪声和观测噪声, 从而导致摄像机的标定精度过度依赖于用户对初始参数的判断和输入以及在噪声环境下鲁棒性较差的问题, 提出了一种基于新息的自适应扩展卡尔曼滤波(AEKF)的摄像机标定优化方法。将二维图像中的特征点坐标作为滤波器的输入, 摄像机的内、外参数的估计值作为滤波器的输出, 将特征点从第 1 个到第  $n$  个进行逐点运算以代替卡尔曼滤波算法中的时间更新, 通过迭代计算得到摄像机的内外参数, 根据摄像机投影模型和自

收稿日期: 2023-06-15; 修回日期: 2023-07-14; 录用日期: 2023-09-06; 网络首发日期: 2023-09-22

基金项目: 国家自然科学基金(62075143)

通信作者: \*zqc@scu.edu.cn

适应扩展卡尔曼滤波算法得到摄像机内、外参数的最优估计值,并且利用重投影误差的大小判断该优化算法的性能。

## 2 摄像机成像模型

摄像机通过成像透镜将目标的三维场景投影到摄像机的二维像平面上,利用摄像机成像模型描述这个变换过程<sup>[1, 22]</sup>。

摄像机成像模型如图 1 所示,其中  $O_w-X_wY_wZ_w$  为三维世界坐标系,  $O_c-X_cY_cZ_c$  为摄像机坐标系,  $O_1(u_0, v_0)$  为成像平面上的主点坐标,空间上任何一点  $P$  在成像平面上的位置可以通过摄像机的成像模型近似表示,即点  $P(x_w, y_w, z_w)$  在成像平面上的位置  $P_u(x_u, y_u)$  为光心  $O_c$  与  $P$  点的连线  $O_cP$  与成像平面的

交点,这种关系也被称为中心射影或透视射影。

空间点从世界坐标系到摄像机坐标系的坐标转换关系式为

$$\begin{bmatrix} x_c \\ y_c \\ z_c \\ 1 \end{bmatrix} = \begin{bmatrix} R & T \\ 0 & 1 \end{bmatrix} \begin{bmatrix} x_w \\ y_w \\ z_w \\ 1 \end{bmatrix} = \begin{bmatrix} r_1 & r_2 & r_3 & t_x \\ r_4 & r_5 & r_6 & t_y \\ r_7 & r_8 & r_9 & t_z \\ 0 & 0 & 0 & 1 \end{bmatrix} \begin{bmatrix} x_w \\ y_w \\ z_w \\ 1 \end{bmatrix}, \quad (1)$$

式中:  $(x_c, y_c, z_c)$  是目标点  $P$  的摄像机三维坐标;  $R$  和  $T$  分别为世界坐标系  $O_w-X_wY_wZ_w$  和摄像机坐标系  $O_c-X_cY_cZ_c$  之间的旋转矩阵和三维平移向量,  $R =$

$$\begin{bmatrix} r_1 & r_2 & r_3 \\ r_4 & r_5 & r_6 \\ r_7 & r_8 & r_9 \end{bmatrix}, T = \begin{bmatrix} t_x \\ t_y \\ t_z \end{bmatrix}。采用单位四元数  $(q_0, q_1, q_2, q_3)$$$

来表示旋转矩阵  $R$ :

$$R = \begin{bmatrix} r_1 & r_2 & r_3 \\ r_4 & r_5 & r_6 \\ r_7 & r_8 & r_9 \end{bmatrix} = \begin{bmatrix} q_0^2 + q_1^2 - q_2^2 - q_3^2 & 2(q_1q_2 - q_0q_3) & 2(q_1q_3 + q_0q_2) \\ 2(q_1q_2 + q_0q_3) & q_0^2 - q_1^2 + q_2^2 - q_3^2 & 2(q_2q_3 - q_0q_1) \\ 2(q_1q_3 - q_0q_2) & 2(q_2q_3 + q_0q_1) & q_0^2 - q_1^2 - q_2^2 + q_3^2 \end{bmatrix}, \quad (2)$$

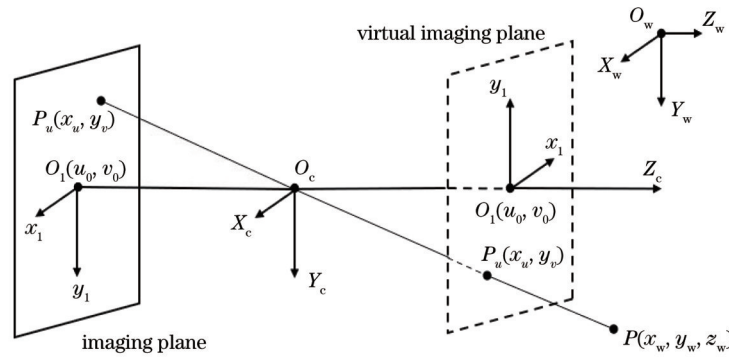


图 1 摄像机成像模型

Fig. 1 Camera imaging model

其中

$$q_0^2 + q_1^2 + q_2^2 + q_3^2 = 1. \quad (3)$$

成像平面坐标与摄像机坐标之间的关系为

$$\begin{bmatrix} x_u \\ y_u \end{bmatrix} = \begin{bmatrix} a_x x_c / z_c + u_0 \\ a_y y_c / z_c + v_0 \end{bmatrix}, \quad (4)$$

式中:  $a_x$  和  $a_y$  分别为  $x$  方向和  $y$  方向上的尺度因子, 或称为归一化焦距;  $(u_0, v_0)$  为主点坐标。

## 3 自适应扩展卡尔曼滤波算法

### 3.1 系统的状态模型

将特征点从第 1 个到第  $n$  个进行逐点运算, 逐点运算过程中的每一步为 EKF 的时间更新<sup>[18]</sup>。设摄像机的内、外参数  $\mathbf{x}_k = [q_0, q_1, q_2, q_3, t_x, t_y, t_z, a_x, a_y, u_0, v_0]^T$  为状态向量,  $k$  为特征点步数索引, 初始化状态量及状态估计误差协方差分别为

$$\begin{cases} \hat{\mathbf{x}}_{00} = E(\mathbf{x}_0) \\ \mathbf{P}_{00} = E[(\mathbf{x}_0 - \hat{\mathbf{x}}_{00})(\mathbf{x}_0 - \hat{\mathbf{x}}_{00})^T] \end{cases}, \quad (5)$$

式中:  $\hat{\mathbf{x}}_{00}$  和  $\mathbf{P}_{00}$  分别为第 0 步的状态估计值和状态估计误差协方差矩阵;  $\mathbf{x}_0$  为状态量初值。

摄像机模型的状态方程为

$$\begin{cases} \hat{\mathbf{x}}_k^- = \Phi_{k-1} \hat{\mathbf{x}}_{k-1}^+ \\ \mathbf{P}_k^- = \Phi_{k-1} \mathbf{P}_{k-1}^+ \Phi_{k-1}^T + \mathbf{Q}_{k-1} \end{cases}, \quad (6)$$

式中:  $\hat{\mathbf{x}}_k^-$  为第  $k$  步的先验状态估计;  $\hat{\mathbf{x}}_{k-1}^+$  为第  $k-1$  步的后验状态估计;  $\mathbf{P}_k^-$  为先验协方差矩阵;  $\mathbf{P}_{k-1}^+$  为  $k-1$  步的后验协方差矩阵;  $\mathbf{Q}_{k-1}$  为过程噪声;  $\Phi_{k-1}$  是一个  $11 \times 11$  的状态转移矩阵, 因为所有特征点都来自同一张目标图像, 所以特征点所对应的内、外参数(状态量)是不变的,  $\Phi_{k-1} = I$  为一个  $11 \times 11$  的单位矩阵。

### 3.2 系统的测量模型

在摄像机标定的过程中, 特征点在图像上的投影坐标  $(x_u, y_u)$  及其对应的世界坐标  $(x_w, y_w, z_w)$ 、四元数

的约束条件  $q_0^2 + q_1^2 + q_2^2 + q_3^2 = 1$  为已知量。将特征点的投影坐标  $(x_u, y_v)$  作为扩展卡尔曼滤波算法的观测值  $z_1, z_2, \dots, z_k$ , 则系统的测量方程可表示为

$$\begin{cases} h_1(k) = a_x(k) \frac{r_1(k)x_w + r_2(k)y_w + r_3(k)z_w + t_x(k)}{r_7(k)x_w + r_8(k)y_w + r_9(k)z_w + t_z(k)} + u_0(k) = x_u(k) \\ h_2(k) = a_y(k) \frac{r_4(k)x_w + r_5(k)y_w + r_6(k)z_w + t_y(k)}{r_7(k)x_w + r_8(k)y_w + r_9(k)z_w + t_z(k)} + v_0(k) = y_v(k) \\ h_3(k) = q_0^2 + q_1^2 + q_2^2 + q_3^2 = 1 \end{cases} \quad (8)$$

$$H_k \approx \frac{\partial h_k(x_k)}{\partial x_k}, \quad (9)$$

式中:  $H_k$  为第  $k$  步测量函数的 Jacobian 矩阵。

### 3.3 更新方程

EKF 的滤波需根据不同的应用场景选择较正确的观测噪声协方差矩阵  $R_k$  和过程噪声协方差矩阵  $Q_k$ 。  $Q_k$  通常被指定为一个基于测量仪器精度的常数矩阵, 而  $R_k$  的选择则采用试错方法, 所以如何不需要人工干预、准确地确定  $R_k$  和  $Q_k$  是滤波效果的关键。本文使用新息自适应地估计协方差矩阵  $R_k$  和  $Q_k$  [23-25], 协方差匹配法根据新息对其协方差矩阵进行调整。EKF 预测过程就是用实际测量值与预测值之间的新息来调整其协方差矩阵, 新息可表示为

$$\epsilon_k = z_k - H_k \hat{x}_k^- \quad (10)$$

引入遗忘因子  $\alpha, \beta$  自适应估计  $R_k$  和  $Q_k$ ,  $\alpha, \beta$  越大则对  $R_k$  和  $Q_k$  初值的权重越大, 反之  $R_k$  和  $Q_k$  自适应估计的权重越大。  $R_k$  和  $Q_k$  可分别表示为

$$\begin{cases} R_k = \alpha R_{k-1} + (1 - \alpha)(\epsilon_k \epsilon_k^T + H_k P_k^- H_k^T) \\ Q_k = \beta Q_{k-1} + (1 - \beta)(K_k \epsilon_k \epsilon_k^T K_k^T) \end{cases}, \quad (11)$$

式中:  $K_k$  为卡尔曼增益;  $\alpha, \beta$  的取值在  $(0, 1]$  区间。利用观测值与经先验估计后的预测值的差值计算状态参数的后验估计 [26], 量测更新方程为

$$\begin{cases} K_k = P_k^- H_k^T (H_k P_k^- H_k^T + R_k)^{-1} \\ \hat{x}_k^+ = \hat{x}_k^- + K_k (z_k - H_k \hat{x}_k^-) \\ P_k^+ = (I - K_k H_k) P_k^- \end{cases}, \quad (12)$$

其中上标“-”和“+”分别表示先验与后验估计。

AEKF 和 EKF 都需要对  $R_k$  和  $Q_k$  输入初值  $R_0$  和  $Q_0$ , 不同的是 EKF 的  $R_k$  和  $Q_k$  在估计过程中是一个常数, AEKF 的  $R_k$  和  $Q_k$  在每次迭代中都会随着新息的变化而更新, 其算法流程如图 2 所示。

## 4 仿真

为验证 AEKF 算法对摄像机标定优化的有效性, 在 Matlab 中根据摄像机投影模型搭建了虚拟摄像机, 虚拟摄像机的内外参数真实值分别为:  $a_x = 1153.9445$ ,

$$z_k = [h_1(k) h_2(k) h_3(k)]^T + [n_1(k) n_2(k) n_3(k)]^T = h_k(x_k) + n_k, \quad (7)$$

式中:  $n_k$  是高斯白噪声,  $n_k = [n_1(k) n_2(k) n_3(k)]^T$ ;  $h_k(x_k)$  为非线性观测模型,  $h_k(x_k) = [h_1(k) h_2(k) h_3(k)]^T$ , 可由投影模型得到 [18-19]:

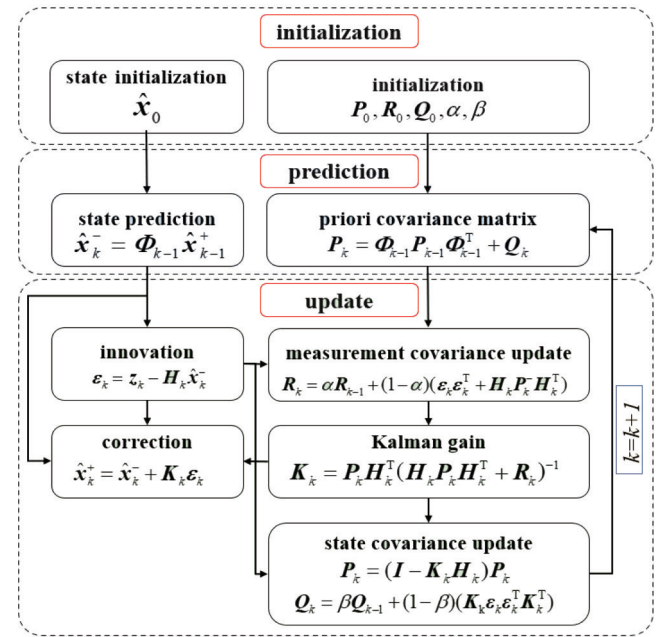


图 2 AEKF 算法流程图

Fig. 2 Flowchart of AEKF algorithm

$a_y = 1153.6987$ , 主点坐标  $(u_0, v_0) = (641.4932, 366.4702)$ , 旋转矩阵的单位四元数  $q_0 = 0.9998, q_1 = 0.0137, q_2 = -0.0078, q_3 = -0.0102$ , 平移矩阵  $T = [-111.3161 \ -73.3006 \ 609.3898]^T$ 。利用 10 组位姿不同、大小为  $13 \times 9$ 、间距为 20 mm 的共面三维坐标点 ( $z$  值均为 0) 通过虚拟摄像机生成虚拟棋盘格标靶, 每张虚拟标靶有  $11 \times 7$  个特征点, 图 3 所示为 10 张位姿不同的模拟标靶。

将生成的 10 张虚拟棋盘格标靶通过张正友标定法得到所设置虚拟相机的内、外参数, 将此内、外参数作为 EKF 和 AEKF 算法的初值。考虑模拟真实标定情况下的特征点提取过程中不可避免地存在误差, 在 EKF 和 AEKF 算法中引入标准差为 0.5 pixel 的随机高斯噪声。虚拟摄像机标定的优化结果如表 1 所示。从表 1 可以看出, 与所设虚拟摄像机内、外参数真实值对比, 经过 AEKF 算法优化后的虚拟摄像机标定结果



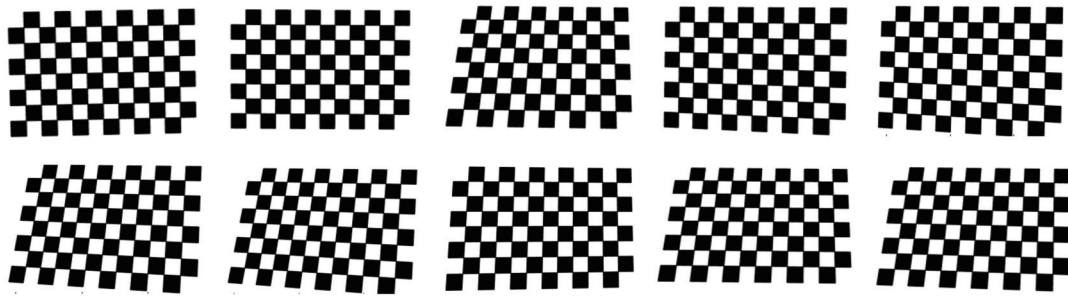


图 3 虚拟棋盘格标靶

Fig. 3 Virtual checkerboard targets

表 1 仿真系统标定结果

Table 1 Calibration results of simulation system

Parameter	Zhang's method	EKF	AEKF
$a_x$ /pixel	1154.0121	1154.0166	1154.0136
$a_y$ /pixel	1153.9131	1153.9169	1153.9312
$u_0$ /pixel	641.9936	641.9652	641.9576
$v_0$ /pixel	367.4038	367.3713	367.2939
$q_0$	0.9998	0.7056	0.7058
$q_1$	0.0140	0.0242	0.0104
$q_2$	-0.0078	0.0001	-0.0013
$q_3$	-0.0102	-0.0071	-0.0068
$t_x$ /mm	-111.3109	-111.3639	-111.3772
$t_y$ /mm	-73.5315	-73.5921	-73.7384
$t_z$ /mm	609.4127	609.3972	609.3762
Reprojection error /pixel	0.7083	0.6794	0.4499

的重投影误差明显小于张正友标定法和 EKF 算法, AEKF 算法优化对虚拟相机的标定精度有一定的提高。

### 5 相机标定优化方法实验

实验采用一个  $12 \times 8$  棋盘作为标定靶, 其中每个小方格的宽度为 20 mm, 以棋盘格的交点作为所提取的特征点, 如图 4 中圆圈所示, 共 77 个。实验使用 USB 摄像机 CAM-OV9714-6 和工业摄像机 BASLER aca1350 进行拍摄以验证所提算法, 所拍摄图像的大小分别为 1280 pixel  $\times$  720 pixel 和 1920 pixel  $\times$  1200 pixel。

为了更加准确地评价滤波效果, 使用重投影误差作为标定效果评价标准。由于观测投影点的图像坐标是直接来自目标图像中提取的, 所以这里将该点称为第一次投影点, 而张正友标定法、UKF、EKF 以及 AEKF 的投影点都是将算法处理后的数据通过摄像机投影模型所得到的, 所以称为重投影点。第一次投影点与重投影点之间的欧氏距离即为重投影误差<sup>[27-31]</sup>。图 5 为重投影误差示意图, 图中  $P$  为三维空间中一点,  $p$  为第一次投影点,  $\hat{p}$  为重投影点,  $p$  与  $\hat{p}$  之间的欧氏距离  $e$  则

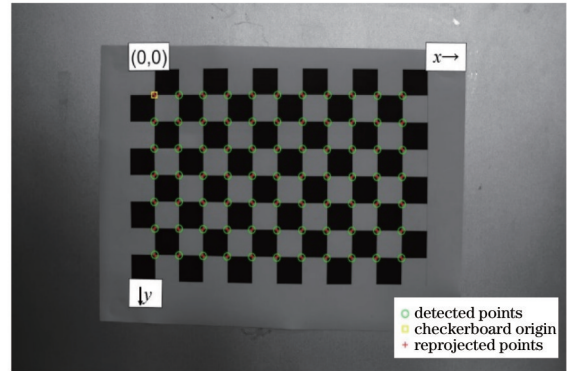


图 4 棋盘格标靶

Fig. 4 Checkerboard target

为重投影误差。

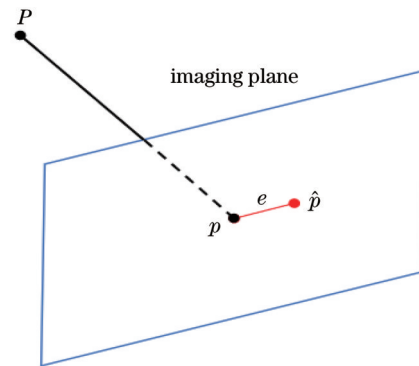


图 5 重投影误差示意图

Fig. 5 Schematic diagram of reprojection error

#### 5.1 USB 相机实验

使用 USB 摄像机拍摄目标棋盘获得 1 组 (10 张) 照片, 通过张正友摄像机标定法获得摄像机的内部参数和外部参数, 将内、外参数作为滤波器的状态量输入。

为验证算法的先进性, 分别采用 UKF、EKF 和 AEKF 对内、外参数进行滤波实验。根据多次试错设置观测噪声误差协方差矩阵, UKF 的  $R_k$  初值设置为  $R_{k00} = [10^2, 0; 0, 13^2]$ , EKF 和 AEKF 的  $R_k$  初值设置为  $R_{k00} = [30^2, 0; 0, 13^2]$ , 过程噪声误差协方差矩阵的初值  $Q_{k00}$  设置为一个  $11 \times 11$  的零矩阵。从拍摄的第 1 张照片中提取 77 个特征点的图像坐标作为 UKF、EKF

和 AEKF 的观测量, UKF、EKF 和 AEKF 分别对输入的张正友标定法得到的摄像机内外参数迭代 77 次, 得

到的实验结果如表 2 所示。由于 UKF 的  $\beta$  值对滤波结果影响较大, 本文选择  $\beta = 1.6$  进行 UKF 实验<sup>[17, 32]</sup>。

表 2 USB 摄像机标定结果  
Table 2 Calibration results of USB camera

Parameter	Zhang's method	UKF	EKF	AEKF
$a_x$ / pixel	1149.0384	1149.0259	1149.0400	1149.0490
$a_y$ / pixel	1149.2140	1149.2233	1149.2087	1149.2018
$u_0$ / pixel	628.0821	628.1140	628.0701	628.0812
$v_0$ / pixel	378.5566	378.5508	378.5822	378.5690
$q_0$	0.9997	0.9982	0.7054	0.7059
$q_1$	0.0217	-0.0028	0.0277	0.0113
$q_2$	0.0022	-0.0191	-0.0004	-0.0072
$q_3$	-0.0100	-0.0097	-0.0065	-0.0069
$t_x$ / mm	-103.9589	-103.8969	-103.9813	-103.9627
$t_y$ / mm	-79.8024	-79.8154	-79.7535	-79.7688
$t_z$ / mm	605.5485	605.5545	605.5555	605.5527
Reprojection error / pixel	0.8284	0.5264	0.6381	0.3217

从表 2 中的重投影误差可以看出, 三种算法均提升了标定精度, UKF、EKF 和 AEKF 算法相对于张正友标定法精度分别提升了 36.46%、22.97% 和 61.17%。UKF 和 EKF 算法对优化结果有一定的提高, 但 AEKF 算法的提升较为明显。为了更加直观地看出滤波效果, 绘制目标图像的实际投影点、张正友标定法重投影点、UKF、EKF 和 AEKF 滤波后的重投影点在同一张图像上, 如图 6 所示, 其中  $x_u$  和  $y_v$  为像素坐标系的横、纵坐标, 可以明显看出 AEKF 的重投影点相对于张正友标定法的重投影点更加靠近实际观测投影点。

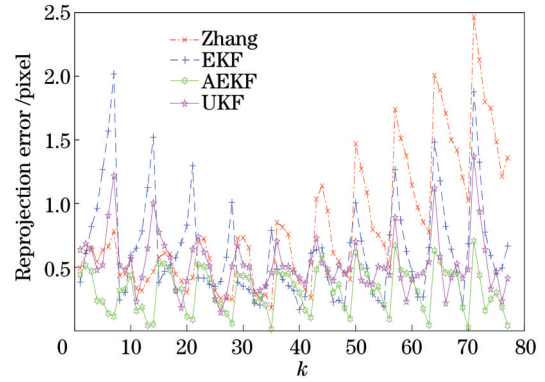


图 7 特征点的重投影误差

Fig. 7 Reprojection error of feature points

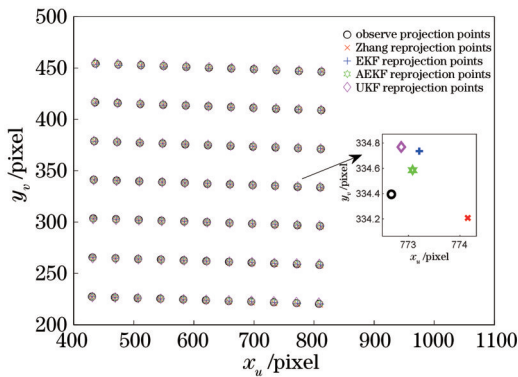


图 6 不同算法的重投影点结果

Fig. 6 Results of reprojection points for different algorithms

77 个特征点经过张正友标定法、UKF、EKF 和 AEKF 算法优化后的重投影误差如图 7 所示。从图 7 中可以看出, AEKF 算法优化后重投影误差整体小于张正友标定法、UKF、EKF 算法的重投影误差, 只是在个别点处 AEKF 算法的重投影误差略大于 UKF 和 EKF 算法, 并且 AEKF 曲线的波动较小, 说明各个特

征点之间的重投影误差在各个点上的重投影误差较小且相近。

图 8 对比了 UKF、EKF 和 AEKF 算法在滤波过程中的效果, 给出 UKF、EKF 和 AEKF 滤波过程中每一次迭代的重投影误差, 从图 8 可以看出: 经过 UKF、EKF 和 AEKF 算法优化后的摄像机标定重投影误差都随着迭代次数的增加而逐渐收敛, UKF 的收敛速度较慢且收敛曲线波动较大; UKF 和 EKF 由于噪声协方差矩阵的选取是固定值, 在  $k = 8, 15$  以及  $k = 3$  时噪声协方差矩阵的不合适对算法有影响, 曲线出现了较大的振荡, 而 AEKF 算法由于自适应变化噪声协方差矩阵, 其重投影误差相较于 UKF 和 EKF 算法的重投影误差整体较小且曲线振荡幅度更小, 有较高的滤波精度和较好的优化效果。

为了分析所提算法的鲁棒性, 在 UKF、EKF 和 AEKF 的观测量  $(x_u, y_v)$  中加入  $0.1 \sim 2.0$  pixel 的高斯白噪声<sup>[19]</sup>, 将 UKF、EKF 和 AEKF 同时在 20 种不同噪声等级的条件下进行对比实验, 得到三种滤波算法在

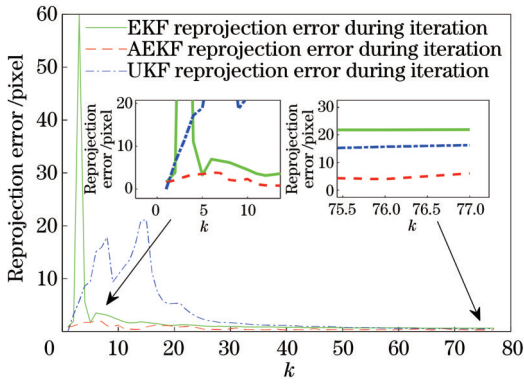


图 8 迭代过程中重投影误差的变化

Fig. 8 Variation of reprojection error during iteration

不同噪声级别下的滤波效果,如图 9 所示。随着噪声等级从 0.1 pixel 到 2.0 pixel 逐渐增加, EKF 和 AEKF 的重投影误差增大,但是 AEKF 相对于 EKF 的重投影误差整体较小且增加缓慢,而 UKF 算法在噪声逐渐增大的环境下,重投影误差迅速增加且整体偏大。

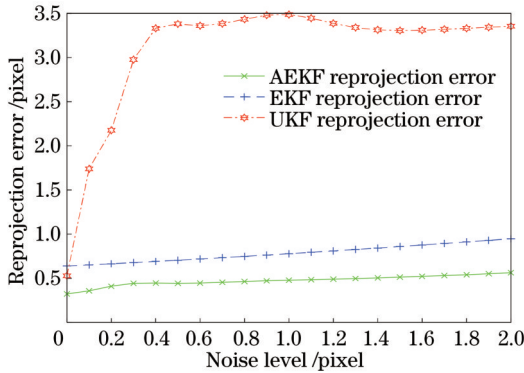


图 9 重投影误差与噪声等级的关系

Fig. 9 Reprojection error varying with noise level

通常情况下 EKF 算法的观测噪声协方差矩阵  $R_k$  的值根据经验和多次试错获得,使滤波器精度达到可接受范围。为了验证 AEKF 算法解决了 EKF 算法依赖于用户对  $R_k$  值的选择问题,本文改变  $R_k$  的初值以测试算法对其设置不具有依赖性,设置  $R_k = j \times R_{k0|0}^2$ , 其中  $j \in (0, 2.0]$ , 得到如图 10 所示的 EKF 和 AEKF 在不同  $R_k$  时的滤波效果图。

从图 10 中可以看出, AEKF 算法的重投影误差随着  $R_k$  的变化呈整体较小且平缓的状态,而 EKF 的重投影误差随着  $R_k$  的变化有较为明显的变化,并且在  $0.1R_k$  处存在较大偏差。这说明 AEKF 算法对  $R_k$  有较好的自适应效果,降低了 EKF 算法精度对  $R_k$  初值的依赖。

### 5.2 工业相机实验

为了进一步验证所提 AEKF 算法对相机标定优化的普适性,实验采用工业相机对目标棋盘格拍摄 1 组(10 张)照片。与 USB 相机实验相同,设 UKF 的观测噪声误差协方差矩阵的初值  $R_{k0|0} = [20^2, 0; 0, 2^2]$ , EKF 和 AEKF 观测噪声误差协

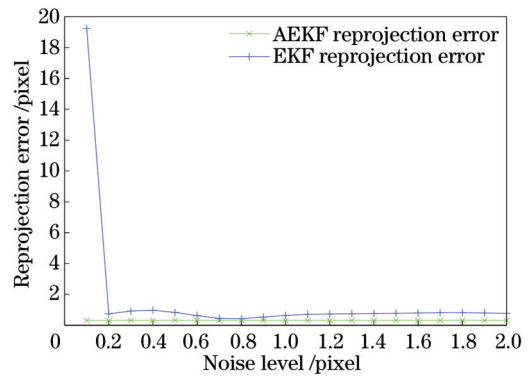


图 10 不同  $R_k$  时标定优化算法的重投影误差

Fig. 10 Reprojection error of calibration optimization algorithm at different  $R_k$

方差矩阵的初值  $R_{k0|0} = [10^2, 0; 0, 30^2]$ , 过程噪声误差协方差矩阵的初值  $Q_{k0|0}$  为一个  $11 \times 11$  的零矩阵。通过张正友摄像机标定法获得工业相机的内部参数和外部参数,并将其作为滤波器状态量。

工业相机标定参数经过 UKF、EKF 和 AEKF 优化后的内、外参数如表 3 所示。从表 3 中重投影误差的大小来看, UKF、EKF 和 AEKF 算法的精度相对于张正友标定法分别提高了约 12.06%、9.76% 和 12.17%。UKF、EKF 和 AEKF 的重投影误差与迭代次数的关系曲线如图 11 所示。与 USB 相机的实验结果类似,工业相机参数的重投影误差在 UKF、EKF 和 AEKF 的滤波过程中随着迭代次数的增加均为收敛状态, UKF 收敛曲线在前期略有振荡, AEKF 相较于 UKF 和 EKF 振荡幅度较小。

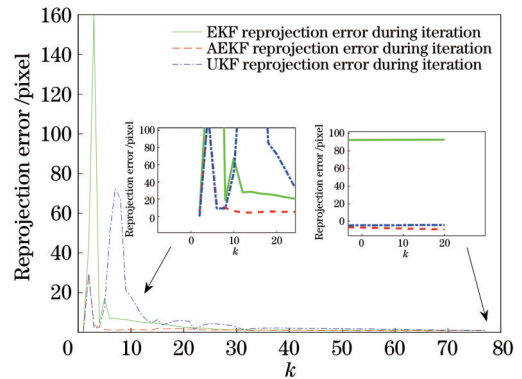


图 11 迭代过程中重投影误差的变化

Fig. 11 Variation of reprojection error during iteration

为了分析算法在工业相机标定优化中的鲁棒性,在 UKF、EKF 和 AEKF 的观测值  $(x_u, y_v)$  中同样引入 0.1~2.0 pixel 的高斯白噪声<sup>[19]</sup>, 将 UKF、EKF 和 AEKF 同时在 20 种不同噪声等级下进行对比实验,得到三种滤波算法在不同噪声级别下的滤波效果,如图 12 所示。从图 12 可以看出,随着噪声等级的逐渐增加, UKF 的重投影误差随着噪声等级的增大波动较大,而 EKF 和 AEKF 的重投影误差呈现先下降后上升



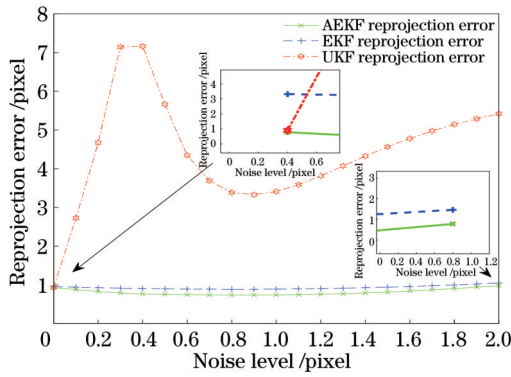


图 12 重投影误差与噪声等级的关系

Fig. 12 Relationship between reprojected error and noise level. The trend shows that the reprojected error of EKF and AEKF increases with the noise level after adding 0.8 pixel Gaussian white noise, and the reprojected error of AEKF is always smaller than that of UKF and EKF, indicating that the AEKF algorithm

is more robust than UKF and EKF algorithms in a noisy environment for camera calibration.

With noise-free conditions, the optimized UKF, EKF, and AEKF parameters are used as reference values. The relative error of the internal and external parameters as the noise level gradually increases is shown in Fig. 13. From Fig. 13, it can be seen that as the noise level increases, the relative error of the translation vector, scale factor, and principal point coordinates after UKF filtering all show significant fluctuations, while the relative error of the results after EKF and AEKF filtering all increase with the noise level. Observing the interval of the relative error of the internal and external parameters, due to the addition of the new information adaptive algorithm, the relative error of the parameters of AEKF is smaller than that of UKF and EKF, and the relative error is within the acceptable error range. From the experiment, it can be seen that the proposed adaptive extended Kalman filtering algorithm has a better inhibitory effect on observation noise. Nonlinear filtering is highly dependent on the initial value, and when the noise changes, the fixed initial value is not conducive to the filtering process. Due to the influence of various factors on the images captured during each calibration, the observation noise

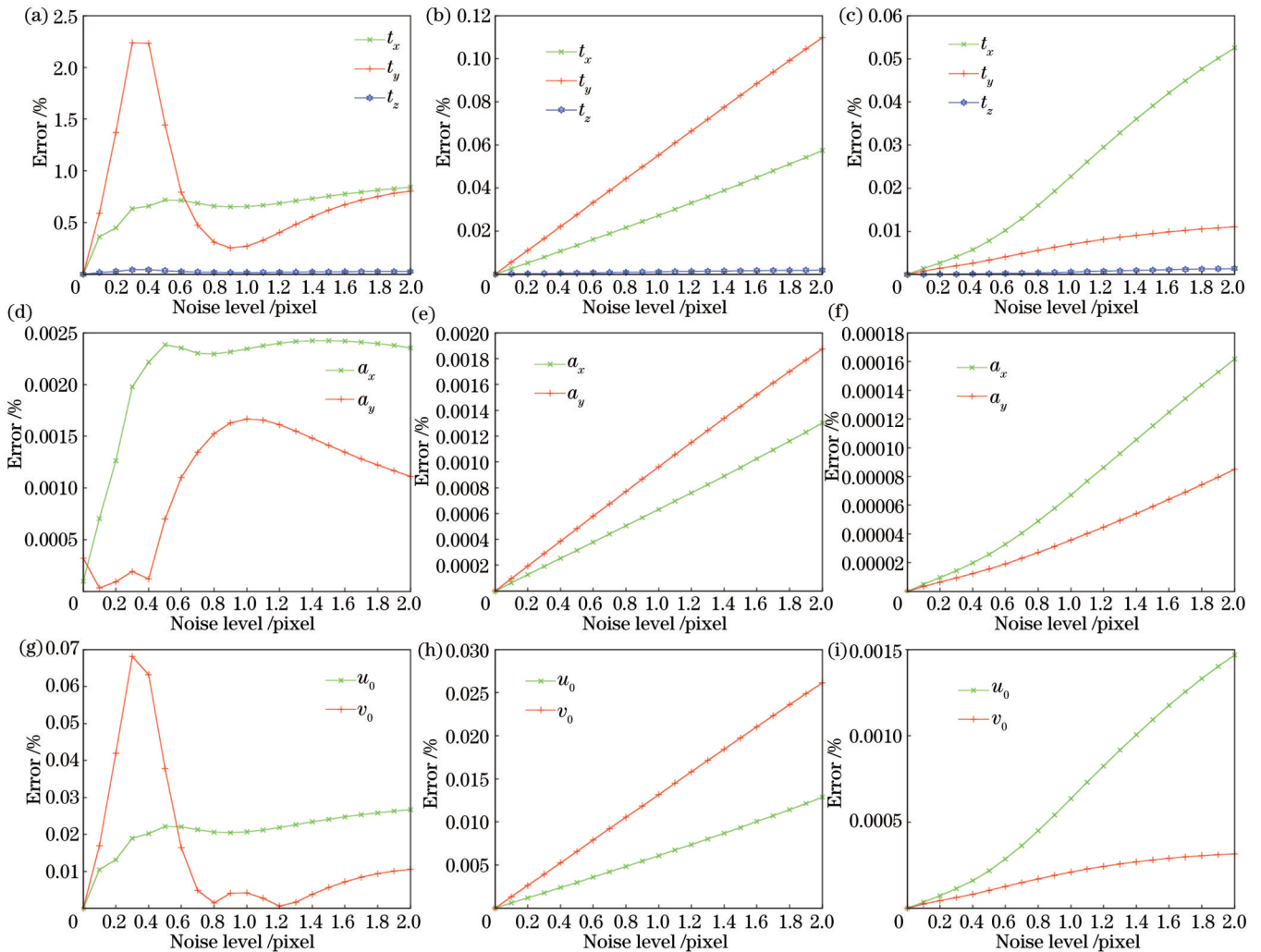


图 13 内、外参数相对误差与噪声等级的关系。平移向量使用(a)UKF、(b)EKF 和(c)AEKF 优化;尺度因子使用(d)UKF、(e)EKF 和(f)AEKF 优化;主点坐标使用(g)UKF、(h)EKF 和(i)AEKF 优化

Fig. 13 Relationship between relative error of intrinsic and extrinsic parameters and noise level. Optimization of translation vector by using (a) UKF, (b) EKF, and (c) AEKF; optimization of scale factor by using (d) UKF, (e) EKF, and (f) AEKF; optimization of principal point coordinate by using (g) UKF, (h) EKF, and (i) AEKF

表 3 工业摄像机标定结果  
Table 3 Calibration results of industrial camera

Parameter	Zhang's method	UKF	EKF	AEKF
$a_x$ /pixel	2789.3876	2789.3780	2789.3780	2789.3807
$a_y$ /pixel	2791.2596	2791.2692	2791.2566	2791.2603
$u_0$ /pixel	935.3057	935.3159	935.3499	935.3353
$v_0$ /pixel	566.0097	565.9948	566.0444	566.0195
$q_0$	0.9993	0.9992	0.7047	0.7047
$q_1$	-0.0134	-0.0187	-0.0121	-0.0153
$q_2$	-0.0311	-0.0379	-0.0286	-0.0282
$q_3$	0.0183	0.0182	0.0125	0.0126
$t_x$ /mm	-111.0329	-110.9932	-110.8443	-110.9072
$t_y$ /mm	-70.6943	-70.7783	-70.5493	-70.6525
$t_z$ /mm	659.3553	659.3533	659.4082	659.3814
Reprojection error /pixel	1.0563	0.9289	0.9532	0.9277

并不是恒定不变的,AEKF能较好地适应不同噪声的摄像机标定工作中,具有良好的鲁棒性。

## 6 结 论

采用自适应扩展卡尔曼滤波算法对摄像机标定的内、外参数进行优化,以目标棋盘格的交点作为二维图像的特征点,建立了以摄像机投影模型建模的自适应扩展卡尔曼滤波算法。过程噪声和观测噪声协方差矩阵都随着迭代过程中新息的变化而更新,不再依赖于用户的经验判断。实验结果表明:AEKF算法是有效可行的,AEKF算法优化后摄像机参数的重投影误差明显小于EKF算法、UKF算法和张正友标定法重投影误差;在噪声逐渐增大的环境下,重投影误差在AEKF算法下相较于UKF和EKF算法整体较小且增加缓慢,AEKF算法具有较高的精度和鲁棒性。

## 参 考 文 献

- [1] 张广军. 机器视觉[M]. 北京: 科学出版社, 2005.  
Zhang G J. Machine vision[M]. Beijing: Science Press, 2005.
- [2] Liu J, Fu W P, Wang W, et al. Accuracy analysis of robot binocular vision calibration[J]. Advanced Materials Research, 2014, 1044/1045: 696-699.
- [3] 张宏峰, 倪受东, 赵亮, 等. 基于麻雀搜索算法的摄像机标定优化方法[J]. 激光与光电子学进展, 2021, 58(22): 2215004.  
Zhang H F, Ni S D, Zhao L, et al. Camera calibration optimization method based on sparrow search algorithm[J]. Laser & Optoelectronics Progress, 2021, 58(22): 2215004.
- [4] 安世勇, 朱江平, 杨红雨, 等. 基于绝对相位靶的摄像机标定仿真与实验研究[J]. 激光与光电子学进展, 2022, 59(4): 0412001.  
An S Y, Zhu J P, Yang H Y, et al. Simulation and experiment research on camera calibration based on absolute phase target[J]. Laser & Optoelectronics Progress, 2022, 59(4): 0412001.
- [5] Kang S, Kim S D, Kim M. Structural-information-based robust corner point extraction for camera calibration under lens distortions and compression artifacts[J]. IEEE Access, 2021, 9: 151037-151048.
- [6] 李铁军, 薛路明, 刘今越, 等. 基于辅助相机的景深拓展三维重建技术研究[J]. 红外与激光工程, 2023, 52(4): 20220647.

- Li T J, Xue L M, Liu J Y, et al. Research on 3D reconstruction technology of extended depth of field based on auxiliary camera [J]. Infrared and Laser Engineering, 2023, 52(4): 20220647.
- [7] 龙陵波, 赵宏, 杨聪, 等. 铁路道岔参数机器视觉在位测量方法与装置[J]. 电子测量与仪器学报, 2023, 37(4): 80-89.  
Long L B, Zhao H, Yang C, et al. Machine-vision based method and apparatus for *in-situ* measurement of railway turnout parameters[J]. Journal of Electronic Measurement and Instrumentation, 2023, 37(4): 80-89.
- [8] 张紫建, 庞茂, 滕传超, 等. 基于线结构光的软包电池表面检测系统研究[J]. 应用激光, 2023, 43(5): 88-93.  
Zhang Z J, Pang M, Teng C C, et al. Research on surface detection system of soft pack batteries based on line structured light[J]. Applied Laser, 2023, 43(5): 88-93.
- [9] 蒋建国, 李相涛, 齐美彬, 等. 基于DSP的变外参摄像机在线标定[J]. 仪器仪表学报, 2008, 29(12): 2617-2621.  
Jiang J G, Li X T, Qi M B, et al. Online calibration of camera with changeable extrinsic parameters based on DSP[J]. Chinese Journal of Scientific Instrument, 2008, 29(12): 2617-2621.
- [10] 胡天策, 蔡俊峰, 徐榕, 等. 基于内窥镜单目视觉手术导航的测距方法[J]. 中国组织工程研究与临床康复, 2008, 12(22): 4241-4245.  
Hu T C, Cai J F, Xu R, et al. Distance measurement based on endoscope with monocular vision[J]. Journal of Clinical Rehabilitative Tissue Engineering Research, 2008, 12(22): 4241-4245.
- [11] 王谭, 王磊磊, 张卫国, 等. 基于张正友标定法的红外靶标系统[J]. 光学精密工程, 2019, 27(8): 1828-1835.  
Wang T, Wang L L, Zhang W G, et al. Design of infrared target system with Zhang Zhengyou calibration method[J]. Optics and Precision Engineering, 2019, 27(8): 1828-1835.
- [12] 贾畅, 卞永鑫, 金伟峰, 等. 一种基于主动式双目视觉的三维测量方法[J]. 仪表技术, 2022(3): 66-71.  
Jia C, Bian Y X, Jin W F, et al. A three-dimensional measurement method based on active binocular vision[J]. Instrumentation Technology, 2022(3): 66-71.
- [13] 赵晓理, 周浦城, 薛模根. 一种用于光电立靶系统的线阵相机现场自标定方法[J]. 光电工程, 2016, 43(7): 59-66.  
Zhao X L, Zhou P C, Xue M G. A kind of linear array camera field self calibration method for electro-optical vertical target system[J]. Opto-Electronic Engineering, 2016, 43(7): 59-66.
- [14] Zhang Z Y. A flexible new technique for camera calibration[J]. IEEE Transactions on Pattern Analysis and Machine Intelligence, 2000, 22(11): 1330-1334.
- [15] Tommaselli A M G, Tozzi C L. Line based camera calibration



- in machine vision dynamic applications[J]. SBA Controle & Automacao, 1999, 10(2): 100-106.
- [16] Stringa E, Regazzoni C S. A novel camera calibration algorithm based on Kalman filter[C]//Proceedings 15th International Conference on Pattern Recognition, September 3-7, 2000, Barcelona, Spain. New York: IEEE Press, 2002: 872-875.
- [17] 陈益, 赵高鹏, 刘娣. 简化 UKF 算法在摄像机标定中的应用[J]. 计算机工程, 2009, 35(19): 274-276.  
Chen Y, Zhao G P, Liu D. Application of simplified UKF algorithm in camera calibration[J]. Computer Engineering, 2009, 35(19): 274-276.
- [18] Zhou F Q, Zhai J, Zhang G J. A camera calibration method based on iterated extended Kalman filter using planar target[J]. Proceedings of SPIE, 2006, 6358: 63581M.
- [19] 翟晋, 周富强, 张广军. 基于卡尔曼滤波的摄像机标定方法[J]. 光电工程, 2007, 34(9): 60-65.  
Zhai J, Zhou F Q, Zhang G J. Camera calibration method based on Kalman filter[J]. Opto-Electronic Engineering, 2007, 34(9): 60-65.
- [20] Ma Z X, Choi J, Liu P P, et al. Structural displacement estimation by fusing vision camera and accelerometer using hybrid computer vision algorithm and adaptive multi-rate Kalman filter[J]. Automation in Construction, 2022, 140: 104338.
- [21] 张彦泽, 于斌超, 马大智, 等. 自适应扩展卡尔曼滤波机械臂末端定位[J]. 组合机床与自动化加工技术, 2022(10): 150-153, 158.  
Zhang Y Z, Yu B C, Ma D Z, et al. Adaptive extended Kalman filter manipulator end positioning[J]. Modular Machine Tool & Automatic Manufacturing Technique, 2022(10): 150-153, 158.
- [22] 马颂德, 张正友. 计算机视觉: 计算理论与算法基础[M]. 北京: 科学出版社, 1998.  
Ma S D, Zhang Z Y. Computer vision: the basis of computing theory and algorithm[M]. Beijing: Science Press, 1998.
- [23] Akhlaghi S, Zhou N, Huang Z Y. Adaptive adjustment of noise covariance in Kalman filter for dynamic state estimation[C]//2017 IEEE Power & Energy Society General Meeting, July 16-20, 2017, Chicago, IL, USA. New York: IEEE Press, 2018.
- [24] Liu J G, Chen X Y. Adaptive Kalman filter based on multiple fading factors for fast in-motion initial alignment with rotation modulation technique[J]. Proceedings of the Institution of Mechanical Engineers, Part G: Journal of Aerospace Engineering, 2022, 236(15): 3281-3292.
- [25] 张雁琦, 张丽敏, 赵志超, 等. 基于自适应扩展卡尔曼滤波的吡啶菁绿药代动力学实验研究[J]. 中国激光, 2020, 47(9): 0907002.  
Zhang Y Q, Zhang L M, Zhao Z C, et al. Experimental study of indocyanine green pharmacokinetics based on adaptive extended Kalman filter[J]. Chinese Journal of Lasers, 2020, 47(9): 0907002.
- [26] 伍雪冬, 王耀南. 基于视觉和扩展卡尔曼滤波的姿势和运动估计新方法[J]. 仪器仪表学报, 2004, 25(5): 676-680, 687.  
Wu X D, Wang Y N. A novel method of pose and motion estimation based on vision and extended Kalman filter[J]. Chinese Journal of Scientific Instrument, 2004, 25(5): 676-680, 687.
- [27] Koide K, Menegatti E. General hand-eye calibration based on reprojection error minimization[J]. IEEE Robotics and Automation Letters, 2019, 4(2): 1021-1028.
- [28] 马清华, 燕必希, 董明利, 等. 最小化重投影误差的手眼标定优化算法[J]. 激光杂志, 2021, 42(1): 104-108.  
Ma Q H, Yan B X, Dong M L, et al. Hand-eye calibration optimization algorithm based on minimizing reprojection error[J]. Laser Journal, 2021, 42(1): 104-108.
- [29] 吕钧瀚, 姜群, 校金友, 等. 大倾角靶标的双目相机高精度标定方法[J]. 光学学报, 2022, 42(23): 2312002.  
Lü J H, Lou Q, Xiao J Y, et al. High-precision calibration method of binocular cameras for large inclination targets[J]. Acta Optica Sinica, 2022, 42(23): 2312002.
- [30] 姜群, 吕钧瀚, 文立华, 等. 基于亚像素边缘检测的高精度相机标定方法[J]. 光学学报, 2022, 42(20): 2012002.  
Lou Q, Lü J H, Wen L H, et al. High-precision camera calibration method based on sub-pixel edge detection[J]. Acta Optica Sinica, 2022, 42(20): 2012002.
- [31] 石世锋, 叶南, 张丽艳. 具有远近视距的两目视觉系统标定技术研究[J]. 光学学报, 2021, 41(24): 2415001.  
Shi S F, Ye N, Zhang L Y. Calibration of two-camera vision system with far and near sight distance[J]. Acta Optica Sinica, 2021, 41(24): 2415001.
- [32] 董月军, 唐英杰, 任宏亮, 等. 基于无迹卡尔曼滤波的 CO-OFDM 系统相位噪声补偿算法[J]. 中国激光, 2017, 44(11): 1106010.  
Dong Y J, Tang Y J, Ren H L, et al. Phase noise compensation algorithm of CO-OFDM system based on unscented Kalman filter[J]. Chinese Journal of Lasers, 2017, 44(11): 1106010.

## Adaptive EKF-Based Camera Calibration Optimization Method

Lai Xin<sup>1,2</sup>, Yang Xiao<sup>2</sup>, Zhang Qican<sup>1\*</sup>

<sup>1</sup>College of Electronics and Information Engineering, Sichuan University, Chengdu 610065, Sichuan, China;

<sup>2</sup>School of Mechanical Engineering, Southwest Petroleum University, Chengdu 610500, Sichuan, China

### Abstract

**Objective** Camera calibration is significant in machine vision and is widely applied to 3D reconstruction, defect detection, visual navigation, etc. To improve the calibration result accuracy for intrinsic and extrinsic parameters, we propose a camera calibration optimization method based on the adaptive extended Kalman filter (AEKF) algorithm. Zhang's calibration method based on a 2D plane target is a commonly adopted camera calibration approach. Kalman filter (KF), extended Kalman filter (EKF), and unscented Kalman filter (UKF) have been introduced to further enhance the accuracy of Zhang's calibration method. The predicted value of the previous moment and observation value of the current moment are employed to accurately predict the state vector, providing an efficient and precise method to estimate the camera calibration state. EKF algorithm linearizes the nonlinear state equation by performing a first-order Taylor

expansion of the nonlinear function and neglecting the other higher-order terms. Some scholars have applied the EKF algorithm to the camera calibration and yielded better calibration results than Zhang's calibration method. The introduction of a state estimation method can improve the camera calibration accuracy. However, the initial parameter setting of process and observation noises in the EKF algorithm, which affects the optimization of the camera calibration parameters, greatly depends on the user's judgment and choice, and has certain limitations and poor robustness in noisy environments. Therefore, we want to propose a method to perform the EKF-based camera calibration method without dependence on the initial parameter setting, update the process and observation noise covariance matrices employing the innovation between the predicted and observed values, and exhibit good robustness in noisy environments.

**Methods** EKF cannot automatically select and adjust the process and observation noises in the camera calibration, which makes the camera calibration accuracy overly dependent on the user's judgment and inputs of the initial parameters. Thus, the innovation between the predicted and observed values is utilized to update the process and observation noise covariance matrices to adaptively adjust the variation of the process and measurement noises. To address the problems of existing methods, we build a camera projection model based on the imaging principle of the lens and develop an adaptive innovation-based EKF camera optimization calibration method. The unit quaternion is adopted to represent the rotation matrix, the intrinsic and extrinsic parameters of the camera are the state vectors, and the image coordinates of the detected feature points on the two-dimensional checkerboard target are the observation vectors to build the process and measurement model of the AEKF algorithm respectively. The extracted feature points are filtered point by point to obtain the optimal estimation of intrinsic and extrinsic parameters of the camera, and the process and observation noise covariance matrices are updated during the iterative process with the change of the innovation. Meanwhile, the reprojection error is utilized to assess the optimization algorithm performance, and different noise levels are added to validate the algorithm robustness. The EKF-based camera calibration optimization method is introduced to solve the problems that nonlinear filtering depends on the initial parameter setting, the fixed initial parameter is unfavorable to the filtering process under noise changes, and the EKF has poor robustness in noisy environments.

**Results and Discussions** The process and observation noises in the captured images vary during the actual calibration. To overcome the limitation of EKF's inability to adaptively adjust the process and observation noises in camera calibration, we design the innovation between predicted and observed values to update the process and observation noise covariance matrices. AEKF algorithm is presented to optimize the intrinsic and extrinsic parameters of the camera, becoming more suitable for actual applications and eliminating the reliance on fixed initial values for the process and observation noises set by human interventions. A virtual camera and a virtual checkerboard target are constructed based on the camera model. The intrinsic and extrinsic parameters of the virtual camera (state vector) and the 2D image coordinates of the feature points (observation vector) are obtained. Additionally, the reprojected error of the proposed AEKF algorithm is lower than that of other methods (Table 1), which improves calibration accuracy for the virtual camera. The experiments are carried out using a USB camera and an industrial camera respectively. The optimized calibration results of the AEKF algorithm exhibit lower reprojection errors (Figs. 8 and 11) and demonstrate faster convergence and smaller oscillations during the iterative process. The proposed AEKF algorithm still has low reprojection error in the case of gradually increasing noise, which indicates that it has high robustness (Figs. 9 and 12). The effectiveness of the AEKF algorithm is verified by simulation and experiments. The calibration results obtained by the USB camera and industrial camera improve by 61.17% and 12.17% compared with Zhang's calibration method respectively. This algorithm outperforms UKF and EKF in noisy environments in calibration accuracy and robustness, making it applicable to various machine vision fields such as 3D reconstruction, visual navigation, robot localization, and defect detection.

**Conclusions** The proposed AEKF algorithm modeled by the camera projection is employed to optimize the intrinsic and extrinsic parameters of camera calibration, which can improve the mapping accuracy between pixel coordinates and world coordinates. Experimental results demonstrate the effectiveness and feasibility of the AEKF algorithm, leading to a reduction in reprojection errors of camera calibration results. The process and observation noise covariance matrices are updated based on the innovation during the iteration process to eliminate the reliance on the user's judgment. The reprojection error of camera parameters using the AEKF algorithm is significantly lower than that of the EKF algorithm and Zhang's calibration method. Meanwhile, the reprojection error of the AEKF algorithm under the environment of gradually increasing noise is generally lower and grows slowly compared with that of UKF and EKF. Additionally, this algorithm has high accuracy and robustness and can enhance the accuracy of the calibration results, providing better assurance for tasks such as image processing, 3D reconstruction, pose estimation, and machine vision.

**Key words** machine vision; camera calibration; extended Kalman filtering; innovation; adaption; reprojection error